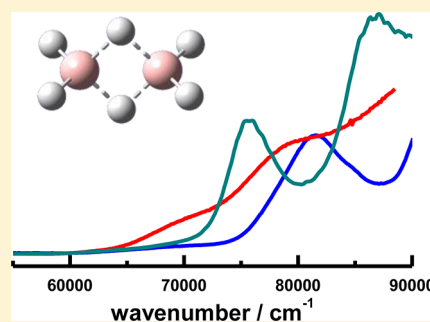


Infrared and Ultraviolet Spectra of Diborane(6): B₂H₆ and B₂D₆Yu-Chain Peng,[†] Sheng-Lung Chou,[†] Jen-Iu Lo,[†] Meng-Yeh Lin,[†] Hsiao-Chi Lu,[†] Bing-Ming Cheng,^{*,†} and J. F. Ogilvie^{*,‡}[†]National Synchrotron Radiation Research Center, 101 Hsin-Ann Road, Hsinchu Science Park, Hsinchu 30076, Taiwan[‡]Escuela de Química, Universidad de Costa Rica, Ciudad Universitaria Rodrigo Facio, San Pedro de Montes de Oca, San Jose 11501-2060, Costa Rica

S Supporting Information

ABSTRACT: We recorded absorption spectra of diborane(6), B₂H₆ and B₂D₆, dispersed in solid neon near 4 K in both mid-infrared and ultraviolet regions. For gaseous B₂H₆ from 105 to 300 nm, we report quantitative absolute cross sections; for solid B₂H₆ and for B₂H₆ dispersed in solid neon, we measured ultraviolet absorbance with relative intensities over a wide range. To assign the mid-infrared spectra to specific isotopic variants, we applied the abundance of ¹¹B and ¹⁰B in natural proportions; we undertook quantum-chemical calculations of wavenumbers associated with anharmonic vibrational modes and the intensities of the harmonic vibrational modes. To aid an interpretation of the ultraviolet spectra, we calculated the energies of electronically excited singlet and triplet states and oscillator strengths for electronic transitions from the electronic ground state.



■ INTRODUCTION

In a probe of the nature of the primary and secondary products of a photochemical reaction, an analysis of their infrared spectra requires a knowledge of the infrared spectra of the precursor or reactant; effective photolytic operations require a knowledge of the ultraviolet spectra of that precursor. For the purpose of our experiments on diborane(6) dispersed in solid neon that yielded our discovery and identification of diborane(4),¹ we hence investigated the infrared and ultraviolet spectra of that parent compound under the most appropriate conditions. The infrared spectra of gaseous and crystalline diborane have been reported in detail,² which led to an empirically derived harmonic or quadratic force field,³ but the published ultraviolet spectra of diborane have poor quality resulting from the primitive conditions of their measurements before year 1950.^{4,5}

For a sample of diborane that contains boron in natural abundance with two stable isotopic variants, 0.801 ¹¹B and 0.199 ¹⁰B, the effective ratio of relative abundance of species ¹¹B₂H₆/¹⁰B¹¹BH₆/¹⁰B₂H₆ is hence about 16:8:1. For diborane dispersed in solid neon at 4 K, the infrared spectral lines are narrow and well resolved, allowing accurate measures of the isotopic shifts from the dominant species, ¹¹B₂H₆, to the isotopic variants ¹⁰B₂H₆ and ¹¹B¹⁰BH₆. In the infrared spectra, the properties of diborane-d₆ are equally important in the analysis of the spectra of its photochemical products with isotopic boron atomic centers in the same proportions. In contrast, the absorption in the ultraviolet region is practically continuous from an apparent onset about 35 000 cm⁻¹ to our limit of observations about 95 000 cm⁻¹; under these conditions quantum-chemical calculations might aid the interpretation of these spectra.

Here we report our analysis of the infrared and ultraviolet absorption spectra of diborane(6) dispersed in solid neon at 4 K and the quantitative ultraviolet spectrum of gaseous diborane, complemented with the aid of quantum-chemical calculations.

■ EXPERIMENTS

For the measurements of infrared absorption spectra, a gaseous sample that was mixed well, containing diborane(6) and neon in great excess, was deposited on a KBr window cooled to 4 K in a closed-cycle cryostat (Janis RDK-415), which was evacuated to less than 1.3 × 10⁻⁶ Pa with a turbomolecular pump backed with a scroll pump.⁶ This cryostat was situated on the plate of a differential rotary-seal stage with rotatable angle 360°; the KBr window can thus be rotated freely to face deposition or photolysis or detection ports. The rate of deposition was regulated between 70 and 130 μL s⁻¹ and monitored with a flow transducer. The duration of deposition was generally 60–180 min. Infrared absorption spectra were recorded with an interferometric infrared spectrometer (Bomem DA8, KBr beamsplitter, HgCdTe detector cooled to 77 K, mid-infrared spectral range 500–5000 cm⁻¹) involving 1000 scans at resolution 0.04 cm⁻¹.

We measured the ultraviolet absorption spectra of gaseous and condensed samples with light from a synchrotron source; the apparatus for this work is described elsewhere.⁷ The ultraviolet light was dispersed with a monochromator (focal length 6 m) on the high-flux cylindrical-grating monochromator (CGM) at beamline BL03 of a storage ring (electron energy 1.5

Received: May 21, 2016

Revised: June 27, 2016

Published: June 28, 2016

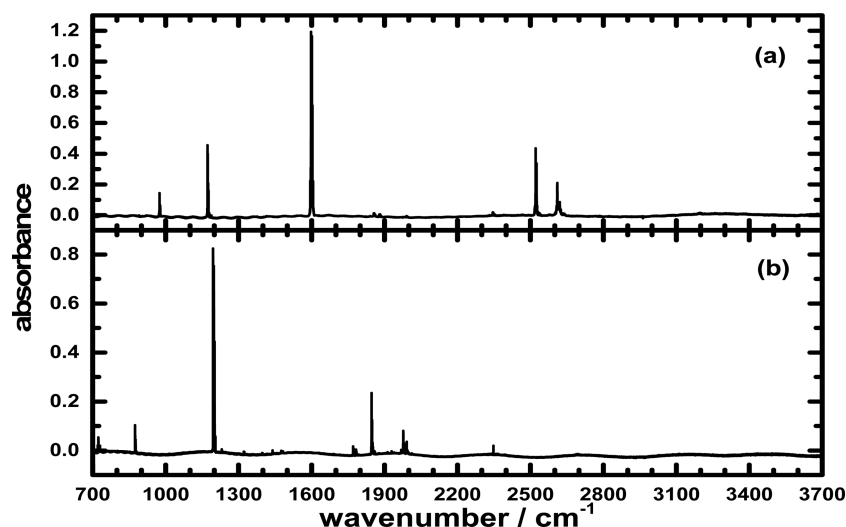


Figure 1. Infrared absorption spectra of diborane(6) dispersed in neon (1:1000) in range 700–3700 cm^{-1} at 4 K for (a) B_2H_6 and (b) B_2D_6 .

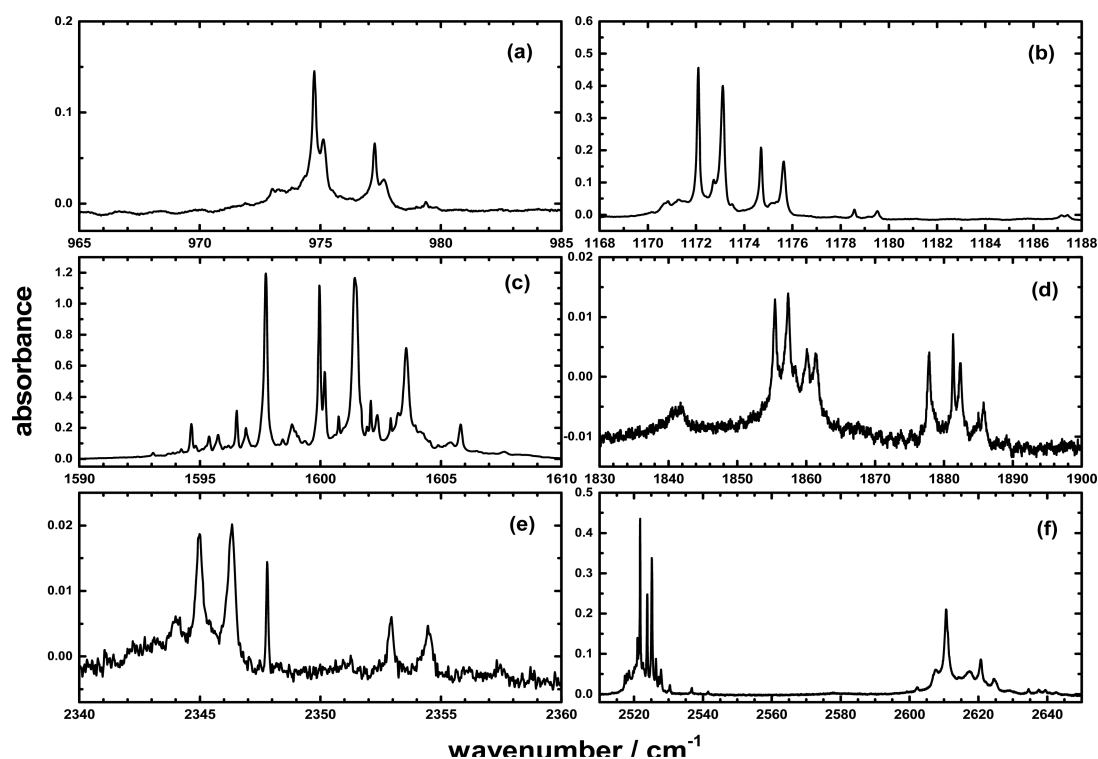


Figure 2. Infrared absorption spectra of B_2H_6 dispersed in neon (1:1000) at 4 K in range/ cm^{-1} (a) 965–985, (b) 1168–1188, (c) 1590–1610, (d) 1830–1900, (e) 2340–2360, and (f) 2510–2650 cm^{-1} .

GeV) named Taiwan Light Source, at National Synchrotron Radiation Research Center (NSRRC). For the gaseous sample, the light passed through an absorption gas cell equipped with two LiF end-windows and was incident on a glass window coated with sodium salicylate; in this work, two gas cells with path lengths of 75.0 and 20.0 mm were used. The converted visible light was measured (photomultiplier tube, Hamamatsu R943-02) in a photon-counting mode. The density of the gas was determined from the pressure recorded with a capacitance manometer (MKS, Baratron) and the temperature monitored with a thermocouple. The absorption was measured at spectral resolution 0.1 nm; the accuracy of the reported spectral positions is ± 0.04 nm.

For the measurements of ultraviolet absorption spectra in a condensed phase, a cryostat was used instead of a gas cell. A gaseous sample was deposited onto a rotatable LiF window maintained about 4 K with another refrigerator system (Janis RDK-415). The transmitted light was incident on a glass window coated with sodium salicylate; the converted visible light was measured with a photomultiplier tube. The gas mixtures were prepared according to standard manometric procedures in a UHV gas-handling system.

Ne (99.999%, Scott Specialty Gases) was used without further purification. B_2H_6 or B_2D_6 (Voltaix, chemical purities B_2H_6 99.99% and B_2D_6 99.8%) was received as 10% in He, which was pumped away at 77 K before use.

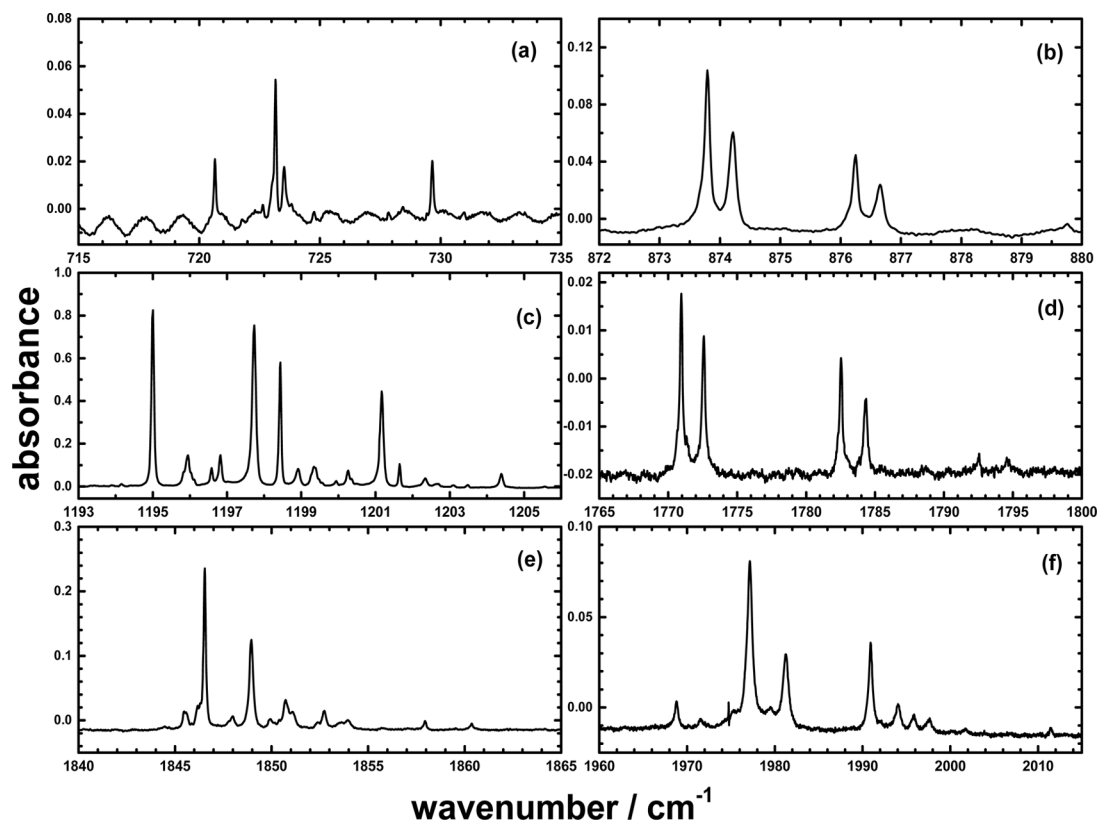


Figure 3. Infrared absorption spectra of B_2D_6 dispersed in neon (1:1000) at 4 K in range/ cm^{-1} (a) 715–735, (b) 872–880, (c) 1193–1206, (d) 1765–1800, (e) 1840–1865, and (f) 1960–2015 cm^{-1} .

CALCULATIONS

The wavenumbers of the harmonic and anharmonic vibrational modes of diborane(6) were calculated with program Gaussian 09,⁸ the B3LYP method, and basis set 6-311++G** (B3LYP/6-311++G**). The vertical singlet and triplet excitation energies of diborane were predicted with two methods, the TDDFT-B3LYP method with aug-cc-pVTZ basis set (TDDFT-B3LYP/aug-cc-pVTZ) and the EOM-CCSD method with 6-311G** basisset (EOM-CCSD/6-311++G**). The singlet and triplet excitation energies were calculated also with program Dalton 2014 with basis aug-cc-pVTZ with a geometry optimized at MC-SCF level.⁹

RESULTS

Analysis of Infrared Spectra of Diborane. Figure 1 shows spectra of B_2H_6 and B_2D_6 over the recorded range, 700–3700 cm^{-1} , in which significant measurable absorption features appear; Figure 2 for B_2H_6 and Figure 3 for B_2D_6 show expanded regions containing notable features. Table 1 presents a list of wavenumbers of absorption lines in infrared spectra of B_2H_6 in its isotopic variants dispersed in Ne at 4 K with a comparison of published data for gaseous and crystalline diborane;² Table 2 presents a similar list for B_2D_6 . Some assignments of combination modes in Table 1 and Table 2 are tentative because the wavenumbers of the modes inactive in infrared absorption are unknowable directly. In specifying these vibrational modes, we apply a systematic sequence according to symmetry classes in order $A_g, A_u, B_{1g}, B_{1u}, B_{2g}, B_{2u}, B_{3g}$, and B_{3u} different from an erratic order used in preceding work.^{2,3} Of 18 fundamental modes of internal vibration expected for a nonlinear molecule comprising eight atomic centers, the

centrosymmetric conformations of $^{10}B_2H_6$ and $^{11}B_2H_6$ at equilibrium according to point group $D_{2h} = V_h$ dictate that nine modes are active in Raman scattering and eight modes in infrared absorption; mode ν_5 , symmetry class A_u , is inactive in either effect. The appearance of many lines interpreted as combinations of modes active in absorption and scattering, however, enables estimates of the participating Raman modes. Although the nuclear arrangement of $^{10}B^{11}BH_6$ according to point group C_{2v} is not centrosymmetric, such that of 18 modes all but 2 of symmetry class A_2, ν_8 and ν_9 , are formally active in infrared spectra, the dissimilarity with $^{11}B_2H_6$ is weak; few of the additional modes might have intensity comparable with the 8 modes of the latter, consistent with our calculations. Our analysis of our newly recorded spectra is assisted by the reported spectra of diborane in both gaseous and crystalline phases for both B_2H_6 and B_2D_6 in natural abundance and ^{10}B enriched to 96%;² these conditions were favorable for the observation of most bands or lines in the active infrared modes in the three species for B with either H or D. As many lines in absorption by B_2H_6 or B_2D_6 dispersed in solid neon have widths comparable with the maximum spectral resolution practicable for our recording of these spectra, a saturation of absorption causes distortion of lines and inaccurate ratios of their statures (net maximum absorbance relative to a baseline); for this reason the apparent ratios of those intensities differ from the formal ratio of relative abundances, but the trends are clear.

Our spectrum of B_2H_6 in natural abundance in solid neon at 4 K displays many absorption features, listed in Table 1, in about 13 distinct sets, classified according to the vibrational modes in the appropriate order according to symmetry species. In many cases, the proximity and ratios of stature enable a clear

Table 1. Wavenumbers/cm⁻¹ of Lines in Infrared Absorption Spectra of B₂H₆ 1:1000 in Ne at 4 K for Indicated Isotopic Variants of B, as ¹⁰B or ¹¹B, Compared with Assigned Modes in Gaseous and Crystalline Phases^{a,b,c}

B ₂ H ₆ in Ne			B ₂ H ₆ gaseous ^b			B ₂ H ₆ crystalline ^b			mode
11,11 ^d	10,11 ^d	10,10 ^d	11,11	10,11	10,10	11,11	10,11	10,10	
920.10	923.98					934	938	940	ν_{13}
974.75	977.25	979.37	972		977	967	970	972	ν_9
975.12	977.64	979.81							
1172.10	1174.71	1178.56	1172		1179	1173	1177	1180	ν_{18}
1172.73	1175.33	1179.14							
1173.11	1175.62	1179.52							
1597.73	1599.96	1602.09	1603		1607	1585	1586	1589	ν_{17}
1601.43	1603.55	1605.81							
1855.48	1857.37	1858.33	1854	1854	1854	1845		1852	$\nu_5 + \nu_{15}$
1860.09	1861.33	1864.06							
1877.87	1882.41	1884.93	1879		1884	1880.4	1883.9	1886.7	ν_8
1881.32	1885.77								
1990.24	1993.65	1996.16							$\nu_{13} + \nu_{15}$
1993.99	1997.63								
2326.02	2329.82								?
2331.34	2334.95								
2344.90	2352.98	2356.17	2343		2355				$\nu_3 + \nu_{18}$
2346.34	2354.44	2357.32							
2373.12	2389.28								$\nu_4 + \nu_{17}$
2380.80	2397.15								
2466.44	2475.77								?
2470.84									
2521.77	2523.84	2526.38	2520		2525	2510.3	2512.4	2515.6	ν_{16}
2525.18	2527.85	2530.38							
2610.62	2620.67	2624.49	2609		2623	2597.1	2607.8	2611.4	ν_{12}

^aA question mark (?) indicates a line or attribution uncertain because of small intensity. ^bFrom ref 2. ^cThe number of the mode as ν_n pertains to ¹¹B₂H₆ unless wavenumbers for only ¹⁰B¹¹B₂H₆ appear in that particular row of the table. ^dRelative statures to the line at 1597.73 cm⁻¹ are listed in Table S7 in Supporting Information.

assignment to triplets of isotopic boron species containing ¹¹B₂, ¹¹B¹⁰B, and ¹⁰B₂, generally in order of increasing wavenumber, although in some cases the small relative abundance of the two carriers ¹⁰B₂H₆ and ¹⁰B₂D₆ precludes the detection of their weakest lines. Apart from the fact that our calculations in Table 3 apply to free molecules whereas our samples for which these spectra are recorded contain diborane molecules constrained within a lattice of neon atoms, the calculated isotopic shifts involving boron nuclei are much better reproduced than the calculated absolute wavenumbers of the lines. A prominent feature in many parts of the spectra of both B₂H₆ and B₂D₆ is the appearance of doublets or triplets of the isotopic triplets. For instance, Figure 2a,b shows two sets of such triplets of B₂H₆ near 975 and 1172 cm⁻¹, assigned to fundamental modes ν_9 and ν_{18} , respectively. The intense features between 1170 and 1180 cm⁻¹, shown in Figure 2b, exhibit an exemplary pattern that is directly assignable as three prominent doublets with relative statures decreasing with increasing wavenumber; two lines of large stature at 1172.1 and 1173.1 cm⁻¹ are attributed appropriately to ¹¹B₂H₆, two lines of moderate stature at 1174.7 and 1175.6 cm⁻¹ are attributed to ¹⁰B¹¹BH₆, and two weak lines at 1178.6 and 1179.5 cm⁻¹ are attributed to ¹⁰B₂H₆. The intervals within the three doublets have mean 0.95 ± 0.04 cm⁻¹. Of the two components of each such doublet, the stature of the line at smaller wavenumber is about 1.1 times that of the line at larger wavenumber. The wavenumber differences of the other two more intense lines from that at 1172.1 cm⁻¹ are 2.6 and 6.4 cm⁻¹; according to Table S3 (Supporting Information), those shifts are calculated to be 2.4 and 6.5 cm⁻¹, respectively, in

satisfactory agreement. Lines at 1172.7, 1175.6, and 1179.1 cm⁻¹ might be additional members that would imply a triplet, rather than a doublet, in each case; these weak lines have a common separation, ~ 0.6 cm⁻¹, from the major lines and consistent ratios of stature. Other weak lines between 1168.27 and 1177.80 cm⁻¹ invoke no obvious assignment; another doublet, barely resolved at 1187.2 and 1187.4 cm⁻¹, is also unassigned, but all these lines might be associated with vibrational mode ν_{18} or combinations of other modes in Fermi resonance thereof.

The region of most intense absorption at about 1600 cm⁻¹, shown in Figure 2c, comprises 34 identified and measured components. Unlike the region near 1175 cm⁻¹, in this case patterns to associate in sets with the isotopic variants are not readily deciphered; Table 1 indicates one plausible doublet for each isotopic variant, whereas 28 lines are left unassigned but all are associated with mode ν_{17} and combinations of other modes that might arise through Fermi resonance. At about 2525 cm⁻¹, three plausible doublets, shown in Figure 2e, are likewise assigned to the isotopic variants but another 18 signals remain unaccounted; all are associated with mode ν_{16} and associated combinations. These three modes ν_{16} , ν_{17} , and ν_{18} belong to symmetry class B_{3u}. Moderately intense lines in two other sets are associated with ν_9 of class B_{1u} and ν_{12} of class B_{2u}. The lines in the latter set at about 2615 cm⁻¹, also shown in Figure 2e, are noticeably broad with widths ~ 1.4 cm⁻¹ at half-maximum stature to be compared with widths ~ 0.22 cm⁻¹ of lines near 2525 cm⁻¹; only a single but broad line is associated with a particular isotopic variant with intervals comparable with those

Table 2. Wavenumbers/cm⁻¹ of Lines in Infrared Absorption Spectra of B₂D₆ 1:1000 in Ne at 4 K for Indicated Isotopic Variants of B, as ¹⁰B or ¹¹B, Compared with Assigned Modes in Gaseous and Crystalline Phases^{a,b}

B ₂ D ₆ in Ne			B ₂ D ₆ gaseous ^b			B ₂ D ₆ crystalline ^b			mode
11,11 ^d	10,11 ^d	10,10 ^d	11,11	10,11	10,10	11,11	10,11	10,10	
	720.65								ν_{13}
723.15	723.52	724.76	722.3		727	718	724.0	722.7	ν_9
873.79	876.25	879.75	873.9	877	880	865.3	867.6	871.4	ν_{18}
874.21	876.65	880.14							
896.20	898.31	901.59							$\nu_{14} + \nu_{15}$
897.10	899.35								
1195.00	1198.44	1201.65	1199.3		1206	1184.9	1188.3	1191.5	ν_{17}
1197.75	1201.17	1204.38							?
	1230.39								
	1233.08								
1321.32	1323.08					1316.5	1316.5	1316.5	$\nu_5 + \nu_{15}$
1322.21	1324.18								
1396.94	1400.40	1404.02							$\nu_{13} + \nu_{15}$
1399.11	1402.47								
1439.23						1424.5	1437.5	1445	$\nu_7 + \nu_{13}$
1475.25	1481.41	1486.90	1477	1484	1489	1476.8	1482.8	1488.3	ν_8
1478.88	1485.09								
1619.25	1633.61					1623	1639	1649	$\nu_3 + \nu_9$
1621.03	1635.04								
1690.74	1694.48	1698.49							
1692.10	1696.06								
1770.91	1782.51	1792.50	1772	1784	1795	1762.2	1774.2	1784.7	$\nu_3 + \nu_{18}$
1771.35	1782.96	1793.00							
1772.57	1784.26	1794.43							
1846.52	1850.74	1857.96			1856	1837.1	1841.3	1849.3	ν_{16}
1848.97	1852.73	1860.37							ν_1
1912.17						1917.2	1926.7	1936.6	$\nu_7 + \nu_{17}$
	1968.84								ν_9
1977.20	1990.91	1997.66	1977		1998	1965.8	1980.3	1986.3	ν_{12}
1981.29	1993.98	2001.68							
2184.37	2195.17	2201.79							$\nu_8 + \nu_{11}$
2188.57	2197.19								
2736.86	2744.06								$\nu_1 + \nu_{18}$
2738.40	2745.40								

^aA question mark (?) indicates a line or attribution uncertain because of small intensity. ^bFrom ref 2. ^cThe numbering of the mode as ν_n pertains to ¹¹B₂H₆ unless wavenumbers for only ¹⁰B¹¹B₂H₆ appear in that particular row of the table. ^dRelative statures to the line at 1195.00 cm⁻¹ are listed in Table S8 in [Supporting Information](#).

in the crystalline phase.² For the lines near 975 cm⁻¹, shown in [Figure 2a](#), three doublets are readily identifiable, with internal separation ~ 0.4 cm⁻¹ and separations 2.5 and 2.1 cm⁻¹ between them consistent with 2.4 and 2.2 cm⁻¹ from calculations and similar intervals for a crystalline sample.² [Figure 2d](#) shows signals between 1850 and 2000 cm⁻¹ in three sets; the sets near 1855 and 1889 cm⁻¹ are attributed to doublets, associated with modes $\nu_5 + \nu_{15}$ and ν_8 , of ¹¹B₂H₆ and ¹⁰B¹¹BH₆; corresponding sets for ¹⁰B₂H₆ are not readily detectable because of small intensity, but the three lines between 1990 and 1998 cm⁻¹ are appropriate as singlets of each isotopic variant, associated with combination mode $\nu_{13} + \nu_{15}$. A barely resolved line at 1993.6 cm⁻¹ provides a hint of further structure in this region but the small ratios of signal to noise preclude definite assignments. Although lines in another seven sets are measurable, their weakness precludes positive identification of lines due to the minor isotopic variant; all firm assignments appear in [Table 1](#); other measured lines are assembled in [Table S1](#) ([Supporting Information](#)). Any line for mode ν_{14} about 370 cm⁻¹ lies beyond our range of detection.

For the region near 1600 cm⁻¹, gaseous B₂H₆ seems to show only one intense vibration–rotational band,² assigned to the most intense fundamental mode ν_{17} , whereas in the spectrum of the crystalline material there likely appear four or five poorly resolved features, depending on the crystalline phase. For our samples of B₂H₆ dispersed in solid neon under conditions in which aggregation of diborane molecules was greatly suppressed through their effective dilution with neon, beyond the two triplets in [Table 1](#) we distinguished 38 components of the absorption between 1593 and 1608 cm⁻¹, listed in [Table S1](#) without attribution to particular isotopic variants, as described above. Similarly in the region near 2520 cm⁻¹, two triplets associated with mode ν_{12} are readily attributed to isotopic carriers containing ¹¹B₂, ¹⁰B¹¹B, and ¹⁰B₂ but another 20 components of the total absorption remain unassigned between 2509 and 2542 cm⁻¹. In the preceding work, the influence of Fermi resonance was considered qualitatively but that interaction fails to provide an accurate explanation of the extent or nature of our data. Because our samples of B₂H₆ and B₂D₆ have great nominal purity, it seems unlikely that other

Table 3. Calculated Data of Diborane(6) (Point Group $D_{2h} = V_h$), $\Delta H_f = 50.1 \text{ kJ mol}^{-1}$, Calculated Wavenumber/ cm^{-1} and Intensity/ km mol^{-1} (in Parentheses) of Vibrational Modes for Various Isotopic Diborane(6)

mode (sym)	$^{11}\text{B}_2\text{H}_6 (D_{2h})$		$^{10}\text{B}_2\text{H}_6 (D_{2h})$		mode (sym)	$^{11}\text{B}^{10}\text{BH}_6 (C_{2v})$	
	calc/ cm^{-1} (int) ^a	calc/ cm^{-1b}	calc/ cm^{-1} (int) ^a	calc/ cm^{-1b}		calc/ cm^{-1} (int) ^a	calc/ cm^{-1b}
$\nu_1 (A_g)$	2524.4 (0)	2518.4	2530.4 (0)	2524.4	$\nu_1 (A_1)$	2528.1 (6.12)	2522.2
$\nu_2 (A_g)$	2094.4 (0)	2100.8	2095.2 (0)	2101.2	$\nu_2 (A_1)$	2513.3 (146.2)	2508.8
$\nu_3 (A_g)$	1159.9 (0)	1164.3	1165.4 (0)	1169.0	$\nu_3 (A_1)$	2095.9 (0)	2101.8
$\nu_4 (A_g)$	770.1 (0)	760.9	801.4 (0)	790.4	$\nu_4 (A_1)$	1648.7 (475.0)	1532.2
$\nu_5 (A_u)$	820.5 (0)	817.8	820.5 (0)	817.7	$\nu_5 (A_1)$	1163.7 (7.07)	1167.6
$\nu_6 (B_{1g})$	2596.2 (0)	2577.3	2611.6 (0)	2591.6	$\nu_6 (A_1)$	1153.5 (68.1)	1159.4
$\nu_7 (B_{1g})$	905.2 (0)	910.5	918.8 (0)	924.4	$\nu_7 (A_1)$	787.0 (0.04)	776.8
$\nu_8 (B_{1u})$	1914.4 (8.80)	1816.9	1925.1 (9.25)	1823.5	$\nu_8 (A_2)$	989.5 (0)	973.2
$\nu_9 (B_{1u})$	958.5 (16.6)	966.9	963.3 (16.7)	971.4	$\nu_9 (A_2)$	820.8 (0)	818.1
$\nu_{10} (B_{2g})$	1784.0 (0)	1695.2	1786.3 (0)	1706.0	$\nu_{10} (B_1)$	1921.2 (8.92)	1821.4
$\nu_{11} (B_{2g})$	863.1 (0)	846.4	878.1 (0)	861.0	$\nu_{11} (B_1)$	1786.6 (0)	1703.9
$\nu_{12} (B_{2u})$	2610.9 (185.5)	2594.9	2626.3 (187.7)	2613.1	$\nu_{12} (B_1)$	961.1 (16.63)	969.3
$\nu_{13} (B_{2u})$	917.2 (0.20)	915.1	921.6 (0.21)	919.7	$\nu_{13} (B_1)$	870.9 (0.03)	854.2
$\nu_{14} (B_{2u})$	346.8 (16.4)	328.3	346.8 (16.4)	328.4	$\nu_{14} (B_2)$	2622.0 (158.3)	2605.9
$\nu_{15} (B_{3g})$	989.6 (0)	974.0	989.6 (0)	973.8	$\nu_{15} (B_2)$	2600.7 (28.4)	2586.4
$\nu_{16} (B_{3u})$	2511.3 (148.7)	2506.6	2516.2 (155.7)	2513.5	$\nu_{16} (B_2)$	920.9 (0.18)	919.9
$\nu_{17} (B_{3u})$	1645.3 (472.6)	1529.2	1650.2 (479.7)	1533.4	$\nu_{17} (B_2)$	910.5 (0.04)	914.6
$\nu_{18} (B_{3u})$	1151.0 (76.8)	1157	1157.6 (74.3)	1163.5	$\nu_{18} (B_2)$	346.0 (16.45)	327.6
$\nu_1 (A_g)$	1834.6 (0)	1864.0	1845.2 (0)	1889.8	$\nu_1 (A_1)$	1839.7 (5.90)	1877.0
$\nu_2 (A_g)$	1486.4 (0)	1497.7	1487.4 (0)	1499.1	$\nu_2 (A_1)$	1816.5 (112.6)	1839.1
$\nu_3 (A_g)$	884.9 (0)	898.1	904.0 (0)	923.8	$\nu_3 (A_1)$	1488.4 (0)	1499.7
$\nu_4 (A_g)$	692.6 (0)	694.8	706.2 (0)	709.5	$\nu_4 (A_1)$	1203.8 (268.6)	1153.0
$\nu_5 (A_u)$	580.1 (0)	583.8	580.1 (0)	583.7	$\nu_5 (A_1)$	895.8 (0.20)	912.5
$\nu_6 (B_{1g})$	1948.8 (0)	1950.9	1970.8 (0)	1978.1	$\nu_6 (A_1)$	855.6 (24.75)	866.4
$\nu_7 (B_{1g})$	722.0 (0)	732.5	734.9 (0)	745.6	$\nu_7 (A_1)$	700.3 (0.05)	703.0
$\nu_8 (B_{1u})$	1429.2 (6.77)	1445.1	1444.2 (7.26)	1457.0	$\nu_8 (A_2)$	699.9 (0)	689.4
$\nu_9 (B_{1u})$	707.2 (8.58)	716.6	712.0 (8.61)	721.1	$\nu_9 (A_2)$	580.6 (0)	584.3
$\nu_{10} (B_{2g})$	1279.6 (0)	1224.7	1283.6 (0)	1228.3	$\nu_{10} (B_1)$	1438.7 (6.94)	1452.9
$\nu_{11} (B_{2g})$	706.1 (0)	702.4	722.9 (0)	719.2	$\nu_{11} (B_1)$	1283.1 (0)	1228.1
$\nu_{12} (B_{2u})$	1956.6 (103.9)	1966.1	1977.6 (106.1)	1986.7	$\nu_{12} (B_1)$	718.2 (2.15)	717.8
$\nu_{13} (B_{2u})$	676.1 (0.04)	682.3	680.7 (0.03)	686.9	$\nu_{13} (B_1)$	707.7 (6.48)	713.8
$\nu_{14} (B_{2u})$	244.7 (8.23)	237.5	244.7 (8.23)	237.5	$\nu_{14} (B_2)$	1972.7 (70.2)	1980.5
$\nu_{15} (B_{3g})$	700.5 (0)	690.3	700.5 (0)	690.1	$\nu_{15} (B_2)$	1950.0 (35.0)	1955.8
$\nu_{16} (B_{3u})$	1814.8 (113.5)	1835.4	1822.6 (122.5)	1847.5	$\nu_{16} (B_2)$	728.7 (0)	739.4
$\nu_{17} (B_{3u})$	1199.0 (267.1)	1148.6	1206.0 (271.8)	1154.9	$\nu_{17} (B_2)$	677.5 (0.03)	683.4
$\nu_{18} (B_{3u})$	852.6 (26.2)	863.5	858.7 (24.1)	869.5	$\nu_{18} (B_2)$	244.8 (8.25)	238.1

^aThese wavenumbers/ cm^{-1} and intensities/ km mol^{-1} within parentheses are calculated with density functional method, B3LYP/6-311++G(d,p), in harmonic approximation and scaled by 0.967. ^bThese wavenumbers/ cm^{-1} are calculated in an anharmonic approximation.

compounds present as impurities are responsible for the many unassigned lines.

Like the corresponding spectrum of B_2H_6 in Ne, the spectrum of B_2D_6 in Figure 1b has prominent absorption lines in five sets, plus moderate absorption in lines in two further sets, and other weak lines in more than 10 additional sets. Figure 3c shows that in the most intense set at about 1200 cm^{-1} three doublets, analogous to those of B_2H_6 in Figure 2b, are readily attributed to the three isotopic variants of diborane- d_6 , as presented in Table 2; the intervals within the doublets have a mean of $2.75 \pm 0.01 \text{ cm}^{-1}$, and the separations between the major components of the doublets are 3.4 and 6.6 cm^{-1} , comparable with calculated shifts 4.4 and 6.3 cm^{-1} in Table S4 (Supporting Information). The widths of the main lines at half-maximum stature appear to be of order 0.06 cm^{-1} , so near the nominal spectral resolution 0.04 cm^{-1} as to result in distortion and saturation of intensity. Another 24 weak features are perceptible within this small region, all listed in Table S2 (Supporting Information). The regions of lines in the second

and third most intense sets are adjacent, between 1840 and 2000 cm^{-1} . Near 1850 cm^{-1} , shown in Figure 3e, three doublets are discernible with internal intervals $\sim 2.2 \text{ cm}^{-1}$, as presented in Table 2, although the relative statures of the lines appear not to conform to the appropriate ratios of isotopic abundances; the widths of these lines are about 0.14 cm^{-1} . An additional 13 lines seem to be associated with the same vibrational mode, ν_{16} , and possible combinations in Fermi resonance. In the other set at about 1980 cm^{-1} , shown in Figure 3f, only two doublets are clearly discernible, as presented in Table 2, with a hint of a third doublet for $^{10}\text{B}_2\text{D}_6$. The widths of lines are at least 0.5 cm^{-1} , larger again than lines near 1840 cm^{-1} . Unlike for B_2H_6 , for which combination lines are readily observable at wavenumbers much above those associated with mode ν_{12} , in our spectra of B_2D_6 the only significant line beyond 2012 cm^{-1} , at 2347.8 cm^{-1} , is likely due to impurity CO_2 .

Among the lines near 875 cm^{-1} , shown in Figure 3b, two doublets are clearly discernible with internal intervals 0.42 cm^{-1}

and separation 3.46 cm^{-1} between major components; any prospective third doublet is lost in the noise level. The widths of lines are $\sim 0.09\text{ cm}^{-1}$. For the four narrow lines near 725 cm^{-1} , shown in Figure 3a, no pattern is discernible; the most intense line at 723.15 cm^{-1} is tentatively associated with $^{11}\text{B}_2\text{D}_6$ and a weaker line at 729.64 cm^{-1} with $^{10}\text{B}^{11}\text{BD}_6$, both for ν_9 . For the lines in a weaker set near 1775 cm^{-1} , shown in Figure 3d, two doublets of internal intervals of 1.65 and 1.75 cm^{-1} are clearly observable with a possible major component of a third doublet; the intervals between major lines with smaller ratios of signal to noise are listed in Table 2. Figure 3d shows a similar triplet of triplets of B_2D_6 near 1770 cm^{-1} , assigned to combination mode $\nu_3 + \nu_{18}$, although the intermediate triplet is masked by its proximity to more intense lines in the dominant triplet. As for B_2H_6 , beyond two prominent sets of isotopic triplets for B_2D_6 perceptible for mode ν_{17} another 40 components of the absorption between 1194 and 1237 cm^{-1} are distinguishable but without specific attribution, listed in Table S2 (Supporting Information). For the region at about 1440 cm^{-1} , the spectra of crystalline B_2D_6 seem to require invocation of three combination modes², $\nu_7 + \nu_{13}$, $\nu_9 + \nu_{11}$, $\nu_4 + \nu_9$, but our spectrum presents 15 lines or components of no evident pattern.

To assist our understanding of these spectra, we undertook quantum-chemical calculations of the wavenumbers and intensities of both B_2H_6 and B_2D_6 in all their three isotopic variants involving boron; within a harmonic approximation, we calculated both the wavenumbers and intensities, whereas within an anharmonic approximation comprising the two largest anharmonic contributions no calculation of intensity was practicable. The wavenumbers from the harmonic calculations were scaled with customary factor 0.967 to take roughly into account the anharmonic effects. In Supporting Information, Tables S3 and S4 for B_2H_6 and B_2D_6 present a list of all calculated wavenumbers and intensities resulting from these calculations according to anharmonic approximation, as described above. Apart from the deviations, small or large relative to the accuracy of measurement, between the harmonic and anharmonic wavenumbers, the large range of calculated intensities is most noteworthy, excluding the zero intensity for modes inactive in infrared absorption; for instance, between the intensities of $^{11}\text{B}_2\text{H}_6$ for mode ν_{17} of symmetry class B_{3u} and ν_{13} of class B_{2u} a factor ~ 2400 is calculated. Such a range, extraordinarily large relative to spectra of comparable hydrocarbon molecules, is perceptible in the experimental spectra of both B_2H_6 and B_2D_6 in Figures 1–3. Regarding the intensities, the ratio of intensities of modes ν_8 and ν_9 of $^{11}\text{B}_2\text{D}_6$ is, for instance, calculated to be about 0.5 , but the observed ratio appears to be about 0.1 ; the trend of calculated intensities in general follows qualitatively that of the experimental measurements but not quantitatively. For the isotopic variants containing both ^{10}B and ^{11}B , hence belonging to point group C_{2v} , some modes corresponding to symmetry class A_1 are calculated to have small intensities, although their counterparts for variants with either $^{10}\text{B}_2$ or $^{11}\text{B}_2$ are inactive in infrared absorption; for instance, Table 3 shows that modes $\nu_1 \text{A}_1$, $\nu_5 \text{A}_1$, and $\nu_{15} \text{B}_2$ of $^{10}\text{B}^{11}\text{BH}_6$, which are calculated to have significant intensity, correlate with modes ν_1 , ν_3 and ν_6 , all of symmetry class A_{1g} of $^{11}\text{B}_2\text{H}_6$, which are calculated to have zero intensity. With careful measurement of spectra and great photometric accuracy arising from digital representation of spectra converted from the directly recorded interferograms, we cope with such large ranges of intensities, but the ratio of signal to noise must

eventually affect adversely the detectability of the weakest features when the most intense lines are maintained within a range of photometric accuracy.

In Table S5 (Supporting Information), we compare for dominant isotopic variant $^{11}\text{B}_2\text{H}_6$ the wavenumbers calculated in both harmonic and anharmonic models with the best experimental data for free molecules;³ the mean deviation between observed and calculated wavenumbers of fundamental modes is $+28.8 \pm 30\text{ cm}^{-1}$ for $^{11}\text{B}_2\text{H}_6$ and $+13.8 \pm 18.4$ for $^{11}\text{B}_2\text{D}_6$. The agreement between calculated and observed wavenumbers is clearly only moderate with the discrepancies being much larger than the precision of measurement. Such large and erratic differences are only roughly helpful for the assignment of vibrational modes, but the calculated shifts, as presented in Table S3 and Table S4 (Supporting Information), between $^{11}\text{B}_2\text{H}_6$ or $^{11}\text{B}_2\text{D}_6$ and the other variants are more reliable and have been applied in some assignments in Tables 1 and 2. This comparison in Table S5 is valuable and meaningful not only in its own right within our investigation of this stable compound diborane(6) but also as an indication of what might be expected for a related transient species such as diborane(4)¹ for which well defined conditions of known concentration or isolation from other absorbing species is impracticable.

Analysis of Ultraviolet Spectra of Diborane. We recorded the ultraviolet absorption of diborane B_2H_6 under three conditions, gaseous phase near 298 K with density selected to maintain the absorbance within an appropriate range for optical paths of two lengths, a pure solid film, and a dispersion in solid neon near 4 K . By comparison of those spectra with actual spectra of N_2 , O_2 , H_2O , and CO_2 , we are confident that all perceptible features are due to diborane, not to impurities. Figure 4 presents the absolute cross section for

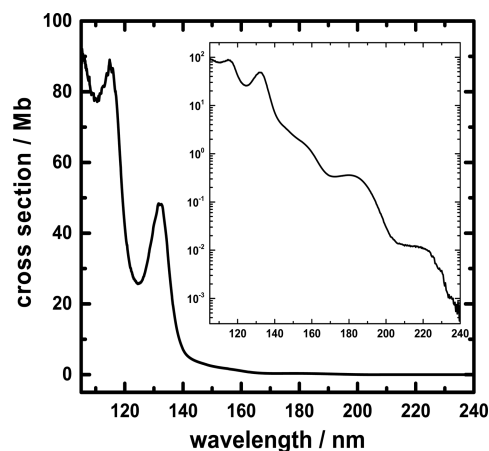


Figure 4. Spectral absorption of gaseous B_2H_6 in the wavelength range 105 – 240 nm with linear and (inset) logarithmic scales of absolute cross section.

the absorption of gaseous B_2H_6 on a wavelength scale with both linear and logarithmic cross sections. Figure 5 presents the same region for gaseous B_2H_6 on a wavenumber scale in two sections because of the great range of the intensity. Under the conditions of our measurements, the absorption becomes perceptible with an onset at about $35\,000\text{ cm}^{-1}$ and increases continuously until the limit of measurements at about $95\,000\text{ cm}^{-1}$ with two local maxima near $76\,000$ and $86\,000\text{ cm}^{-1}$ and a further possible maximum near $55\,000\text{ cm}^{-1}$. Diffuse features at roughly $85\,520$, $86\,350$, $87\,110$, $87\,870$, $88\,810$ and $89\,770$

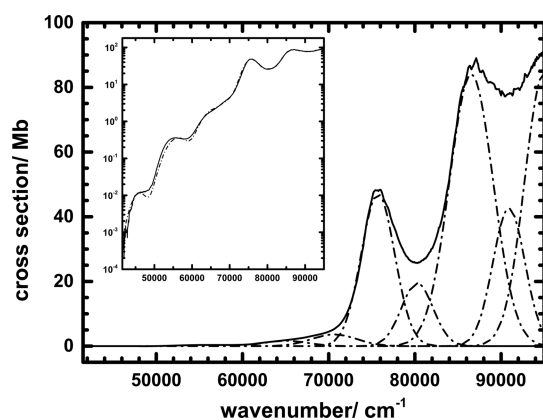


Figure 5. Total absorption and deconvoluted components as absolute cross section of gaseous B_2H_6 in region 41 500–95 000 cm^{-1} ; the full curves are directly measured, the dashed curves in the linear plot indicate the fitted components, and the dashed curve in the inset indicates the sum of absorptions associated with the components. The inset plot has a logarithmic ordinate scale.

cm^{-1} with mean interval $(850 \pm 80) cm^{-1}$ are faintly perceptible above the smoothly varying absorption near the local maximum at about 86 000 cm^{-1} . Associated with a clearly intense electronic transition, that interval is appropriate for a totally symmetric vibrational mode, ν_4 , characterized as B–B stretching and having wavenumber 790 cm^{-1} for $^{11}B_2H_6$ in the electronic ground state.^{2,3} There is otherwise no trace of vibrational structure accompanying the several electronic transitions that must account for the increasingly intense absorption with increasing wavenumber in the ultraviolet region.

To interpret the profile of absorption by means of a deconvolution of the broad features associated with a sequence of electronic transitions, we fitted the observed curve of absorption in Figure 5 to a sum of Gaussian functions with wavenumber of form

$$a\nu \exp\left(\frac{(\nu - b)^2}{c^2}\right)$$

in which ν denotes wavenumber as variable; parameter a is a scaling factor for the total area of a component that has its maximum stature at wavenumber b , and c pertains to the width of that component; pre-exponential factor ν takes into account the frequency factor in absorption spectra at wavenumbers much greater than the equivalent of the temperature of the sample. These fitted components appear also in Figure 5; Figure S1 (Supporting Information) shows the relative residuals to the fit of the spectrum for gaseous B_2H_6 , which indicates the necessity for all 11 components and the quality of the fit. The experimental oscillator strengths are calculated with this formula^{10,11}

$$f = 1.13 \times 10^{-6} \int \sigma \nu d\nu$$

in which the unit of σ is Mb ($= 10^{-22} m^2$) and of ν is cm^{-1} . The results of this deconvolution are presented in Table 4; as the data therein are transcribed directly from the output of the fit, they exhibit insignificant digits but are left without rounding to retain the sense of the fit. Of the 11 components, the fitted widths/ cm^{-1} are roughly constant, 5670 ± 830 , whereas the statures, areas, and oscillator strengths vary over a factor $\sim 30\,000$. Although a visual inspection of the absorption profile might lead one to suspect at least 7 components, 11

Table 4. Fitted Components of Continuous Absorption of Diborane(6) in Gaseous Phase at 296 K and in Solid Phase and Dispersed in Solid Neon at 4 K

component	wavenumber/ cm^{-1}	stature	width/ cm^{-1}	relative area	f value
gaseous B_2H_6					
1	38561 \pm 6	0.0021 \pm 0.0001	5241 \pm 24	11.52 \pm 0.04	0.000013
2	46704 \pm 7	0.0163 \pm 0.0001	5845 \pm 11	101.35 \pm 0.26	0.000115
3	55646 \pm 22	0.2393 \pm 0.0007	6666 \pm 45	1698.32 \pm 11.41	0.001919
4	63264 \pm 20	0.650 \pm 0.0015	6708 \pm 41	4642.96 \pm 30.21	0.005247
5	67167 \pm 14	1.027 \pm 0.046	5764 \pm 44	6303.04 \pm 36.23	0.007122
6	71904 \pm 37	3.359 \pm 0.042	6069 \pm 88	21702.35 \pm 272.52	0.024524
7	75628 \pm 7	25.647 \pm 0.084	4058 \pm 15	110785.81 \pm 362.26	0.125188
8	80052 \pm 15	13.800 \pm 0.062	5961 \pm 53	87566.03 \pm 587.58	0.098950
9	86388 \pm 6	49.749 \pm 0.112	5436 \pm 16	287891.23 \pm 685.05	0.325317
10	90475 \pm 11	26.796 \pm 0.129	4368 \pm 38	124590.47 \pm 821.51	0.140787
11	94739 \pm 46	53.505 \pm 0.282	5737 \pm 100	326730.89 \pm 6597.62	0.369206
solid B_2H_6					
1	55595 \pm 23	0.0093 \pm 0.0001	7600 \pm 61	75.61 \pm 0.50	
2	62175 \pm 31	0.0202 \pm 0.0001	4530 \pm 61	97.62 \pm 1.42	
3	69750 \pm 11	0.2555 \pm 0.0005	7596 \pm 28	2065.99 \pm 6.37	
4	78040 \pm 9	0.7577 \pm 0.0009	8575 \pm 22	6916.71 \pm 15.94	
5	83521 \pm 29	0.4883 \pm 0.0018	7879 \pm 79	4095.02 \pm 37.34	
6	90972 \pm 168	1.5470 \pm 0.0316	10600 \pm 163	17455.62 \pm 616.8	
solid B_2H_6/Ne					
1	55738 \pm 18	0.0150 \pm 0.0001	8055 \pm 59	128.76 \pm 0.73	
2	64956 \pm 17	0.0350 \pm 0.0002	6669 \pm 49	244.88 \pm 1.42	
3	70449 \pm 26	0.0686 \pm 0.0006	6243 \pm 74	455.81 \pm 4.24	
4	82066 \pm 33	1.0878 \pm 0.0039	8656 \pm 40	10022.68 \pm 77.77	
5	93777 \pm 95	2.0285 \pm 0.0312	7188 \pm 100	15522.03 \pm 440.75	

components are required to yield satisfactory relative residuals (Figure S1, Supporting Information). As the data of the components beyond $90\,000\text{ cm}^{-1}$ are highly sensitive to the immeasurable absorption beyond the limit of our observations near $95\,000\text{ cm}^{-1}$, the two components near nominally $90\,500$ and $94\,700\text{ cm}^{-1}$ are defined less accurately than the other nine components.

Figure S2 (Supporting Information) shows the ultraviolet absorption of pure solid diborane(6) as a solid film near 4 K in region/ cm^{-1} of $47\,000\text{--}88\,500$. A fit similar to that for gaseous B_2H_6 yields only six likely components, listed also in Table 4, of which the sixth component with maximum near $92\,000\text{ cm}^{-1}$ is poorly defined because it lies largely beyond the limit of our measurements. The mean width/ cm^{-1} of the first five components, 7350 ± 850 , is significantly larger than the widths of the components of absorption of the gaseous sample. As the thickness of the film was indeterminate, no oscillator strength is calculable for these absorption features.

Figure S3 (Supporting Information) in two parts shows the ultraviolet absorption spectrum of diborane(6) dispersed in solid neon near 4 K; Table 4 presents the fitted components from deconvolution as employed for the spectra of gaseous and solid samples. The last two components, near $87\,000$ and $94\,000\text{ cm}^{-1}$, have again questionable accuracy because of their proximity to the limit of observation. Here the mean width/ cm^{-1} of the first five components is $\sim 7500 \pm 1700$; the large standard deviation results mostly from the exceptional width of the component near $74\,000\text{ cm}^{-1}$, which is otherwise well defined. These widths are apparently comparable with those of components of absorption of pure solid diborane, hence significantly larger than for gaseous diborane.

To facilitate a comparison of the ultraviolet spectra of diborane(6) in the three experimental conditions, we show in Figure 6, the curves for these conditions; in this figure, the

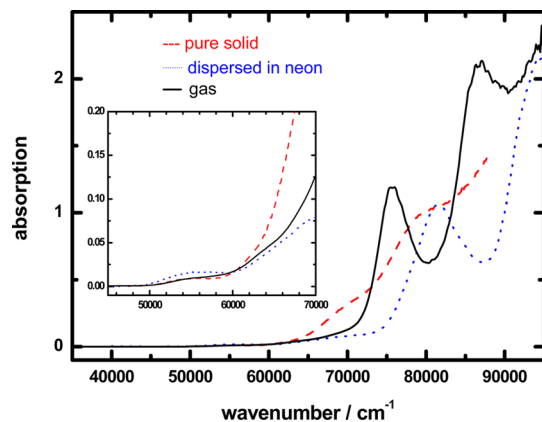


Figure 6. Ultraviolet absorption spectra of gaseous B_2H_6 at 298 K (solid line), pure solid B_2H_6 at 4 K (dashed line), and $\text{B}_2\text{H}_6/\text{Ne} = 1/1000$ at 4 K (dotted line).

ordinate scale is arbitrary but linear, as the absolute intensities for the solid and dispersed samples are unknown. In all three conditions, there is weak absorption with an onset about $50\,000\text{ cm}^{-1}$; Figure 5 clearly exhibits for gaseous B_2H_6 a further diffuse feature with onset near $43\,000\text{ cm}^{-1}$. The local maximum of absorption near $75\,000\text{ cm}^{-1}$ of gaseous B_2H_6 seems to shift near $70\,000\text{ cm}^{-1}$ for the solid phase but in the other direction near $82\,000\text{ cm}^{-1}$ for B_2H_6 dispersed in neon; the local maximum of absorption near $86\,000\text{ cm}^{-1}$ of gaseous

B_2H_6 seems analogously to shift near $78\,000\text{ cm}^{-1}$ for solid B_2H_6 but beyond $93\,000\text{ cm}^{-1}$ for B_2H_6 dispersed in neon. These trends are typical of small molecules between gaseous and condensed phases.

Just as to aid the interpretation of the infrared spectra associated with vibrational transitions in the several isotopic variants we undertook calculations of the wavenumbers and intensities of those transitions, we undertook calculations of electronic transitions from the ground state, a singlet state, to both excited singlet and triplet states with energies up to the ionization energy, $11.38\text{ eV} = 91\,800\text{ cm}^{-1}$, which corresponds roughly to the limit of our observations in the ultraviolet spectrum. All ultraviolet absorption comprises diffuse and almost featureless spectra with intensity in a rapidly increasing trend as one proceeds to greater energy of the excited states. These states must hence be dissociative, which is entirely consistent with the onset of absorption at about $35\,000\text{ cm}^{-1}$ of which the photon energy exceeds that required to dissociate a B–H bond, equivalent to $\sim 32\,500\text{ cm}^{-1}$. The energies calculated for these excited states apply to free molecules, such as in a dilute gaseous phase. For our calculations, we used both Gaussian 9 and Dalton 2014; the pertinent results are presented in Table S6 (Supporting Information).

According to its excitation energy, at about $38\,600\text{ cm}^{-1}$ or 4.78 eV , and its oscillator strength, $f = 1.3 \times 10^{-5}$, the first detected broad absorption in the near-ultraviolet region might mark a transition to a triplet state. Both Gaussian methods indicated such a nearby triplet state of symmetry class B_{3g} near 6.1 eV , but the first triplet state in the Dalton results lies at 7.0 eV . That transition would be made weak not only by the change of multiplicity but also by the symmetry of both states being gerade, that is, $\text{A}_g \rightarrow \text{B}_{3g}$. The other 10 excitations corresponding to the further components of gaseous absorption in Table 4 have oscillator strengths appropriate to transitions to excited singlet states, even though dissociative. For such states the transitions calculated to have significant intensity begin at $8.2\text{ eV} = \sim 66\,000\text{ cm}^{-1}$ from Dalton and $9.0\text{ eV} = \sim 72\,000\text{ cm}^{-1}$ from Gaussian. The oscillator strength, $f \sim 0.027$, calculated for the former transition to state B_{3u} is comparable with that of the fourth component near $65\,000$ or fifth component near $70\,000\text{ cm}^{-1}$. For the further five or six deduced components, their widths combined with the proximity of energies of excited states preclude even tentative correlations. It would seem that for each deduced component of the experimental spectrum two or three calculated states might be involved; the diffuse nature of the absorption prevents more definite assignments.

DISCUSSION

Pertinent to the infrared spectra, a notable feature of the experimental and calculated vibrational transitions is the large range of intensity for fundamental modes, apart from those modes that have zero intensity for reasons of symmetry. Despite this disadvantage, we identified lines of both $^{11}\text{B}_2\text{H}_6$ and $^{11}\text{B}^{10}\text{BH}_6$ dispersed in neon for ν_{13} , but interference from components of much more intense mode ν_9 greatly hindered the identification of the corresponding lines of ν_{13} of B_2D_6 in the same region. Just as we recorded at least 38 components in the vicinity of ν_4 of $^{12}\text{CH}_4$ dispersed in neon near 1300 cm^{-1} ,¹² we counted 44 components in the vicinity of mode ν_{17} of B_2H_6 ; in the latter case, the presence of lines due to three distinct isotopic variants undoubtedly inflates the number of separate transitions with account taken of whatever site effects or

coupling with lattice modes might arise. An advantage of recording spectra of samples at 4 K is that all absorbing molecules are in the vibrational ground state, whereas spectra of gaseous samples² near 298 K might include some detectable absorption features due to transitions of molecules originating in vibrationally excited states.

For these infrared spectra of both B₂H₆ and B₂D₆ dispersed in neon near 4 K, an explanation of either the multiple triplets of lines of isotopic variants or the numerous minor features, in either case associated with a particular vibrational mode, must be speculative, but it is likely that site effects on a molecule embedded within the lattice of neon atoms are at least partially responsible. A diborane molecule is much larger in any physical sense than a single neon atom; a diborane molecule might be expected to occupy the space of at least two adjacent neon atoms. According to the nature of our preparation of the solid samples, rapidly condensed from a stream of gaseous molecules impinging on a surface near 4 K, a rigorously crystalline sample is unlikely, but the spherical nature of the neon atoms must enable a local motion directly on contact with the surface to yield a deposit with at least local crystalline order. Such rapidly condensed samples are known to contain dislocations in large fractions;¹³ such sites provide varied interactions with the diborane molecules therein through the nature of the intermolecular forces in diverse environments. An imposition of larger diborane molecules undoubtedly distorts that local order of neon atomic centers and multiple crystallographically distinct orientations might ensue, leading to the observed multiple isotopic triplets of spectral lines.

Blum and Herzberg claimed to observe⁴ in the ultraviolet region continuous absorption beginning at about 220 nm and increasing toward smaller wavelengths; they expected the absorption to continue, less intensely, to greater wavelengths, which is in agreement with our observations. They claimed also to discern a maximum of absorption about 182 nm = ~55 000 cm⁻¹, which might correlate with our component, of the total profile, deduced at ~54 500 cm⁻¹. Blum and Herzberg discerned no other local maximum of absorption down to 150 nm = ~67,000 cm⁻¹. Price mentioned local maxima of absorption near 135 nm = ~74 000 cm⁻¹ and 120 nm = ~83 000 cm⁻¹,⁵ whereas our accurate photometric measurements and fitted profile indicate major components near ~75 500 and 86 500 cm⁻¹. Given the qualitative nature of the preceding measurements,^{4,5} the agreement is satisfactory.

The significant variation of the form of the ultraviolet absorption spectrum depending on the phase is consistent with our observations for other small molecules, specifically shifts to lesser or greater wavenumbers from the gaseous phase to a condensed phase. The changes observed for B₂H₆ involve shifts of absorption edges and altered intensity patterns. The dominant effect is the increased energy of the excited states relative to the ground state, which is typically associated with greater repulsion between an excited molecule and its neighbors in the constrained space imposed by a lattice, than for a free molecule. A large shift to greater energy might be associated with a transition to a Rydberg state,¹⁴ but our calculations on electronically excited states indicate no strong participation of Rydberg character in the states to which transitions appear to have been recorded, even though the threshold of ionization of a free molecule exists at energies only slightly above the limit of our spectral observations. In the case of a pure solid phase, the interaction of an excited molecule with a neighboring molecule of the same compound might lead

to a partial delocalization of the excitation, yielding a smaller energy than for a free molecule; such a phenomenon might account for the apparent shift of the absorption with maximum near 76 000 cm⁻¹ for the gaseous molecule to about 70 000 cm⁻¹ for solid diborane. As that effect is inoperable for diborane surrounded by neon atoms of which the first electronic excitation occurs at much greater energies, the shift from near 76 000 cm⁻¹ to about 80 000 cm⁻¹ is a more likely explanation. The absence of characteristic vibrational structure accompanying the electronic transitions precludes more definite assignment.

CONCLUSION

Our infrared spectra of diborane, both B₂H₆ and B₂D₆, dispersed in solid neon near 4 K and ultraviolet spectra of diborane B₂H₆ in gaseous and solid phases and dispersed in solid neon represent approximately the state of the art for spectra recorded in those conditions. The widths of infrared spectral lines in the neon matrix are as small as 0.1 cm⁻¹ whereas the widths of deduced components of absorption in the ultraviolet region are as large as 10 000 cm⁻¹, a ratio of order 10⁵. Although the important new knowledge arising from our experiments constitutes the quantitative intensity of ultraviolet absorption of gaseous B₂H₆ and its deconvoluted components, our quantum-chemical calculations related to the energies of electronically excited states, which determine the wavenumbers of transitions from the electronic ground state, and the intensities of those transitions correlate poorly with the experimental data despite that the nature of those calculations represents the extent of accuracy currently attainable with general programs for that purpose. Although the agreement between calculated and observed vibrational features was more satisfactory, there clearly remains much scope also for improved calculations of anharmonic vibrational modes and their intensities.

ASSOCIATED CONTENT

Supporting Information

The Supporting Information is available free of charge on the ACS Publications website at DOI: 10.1021/acs.jpca.6b05150.

The Supporting Information contains additional tables and figures.(PDF)

AUTHOR INFORMATION

Corresponding Authors

*(B.-M.C.) E-mail: bmcheng@nsrrc.org.tw. Tel: +886-3-5780281.

*(J. F.O.) E-mail: ogilvie@cecm.sfu.ca. Tel: 1 778 782-5617.

Notes

The authors declare no competing financial interest.

ACKNOWLEDGMENTS

Ministry of Science and Technology of Taiwan (Grant MOST 102-2113-M-213-005-MY3) and NSRRC provided support of this research. We thank Dr. H.-J. Aa. Jensen of Syddansk Universitet for providing the results of calculations with quantum-chemistry program Dalton.

REFERENCES

(1) Chou, S.-L.; Lo, J.-I.; Peng, Y.-C.; Lin, M.-Y.; Lu, H.-C.; Cheng, B.-M.; Ogilvie, J. F. Identification of Diborane(4) with Bridging B-H-B Bonds. *Chem. Sci.* **2015**, *6*, 6872–6877.

- (2) Duncan, J. L.; McKean, D. C.; Torto, I.; Nivellini, G. D. Diborane: Infrared Spectra of Gaseous and Crystalline Phases, and a Complete Vibrational Assignment. *J. Mol. Spectrosc.* **1981**, *85*, 16–39.
- (3) Duncan, J. L.; Harper, J.; Hamilton, E.; Nivellini, G. D. The Empirical Harmonic Potential Function of Diborane. *J. Mol. Spectrosc.* **1983**, *102*, 416–440.
- (4) Blum, E.; Herzberg, G. On the Ultraviolet Absorption Spectrum of Diborane. *J. Phys. Chem.* **1937**, *41*, 91–95.
- (5) Price, W. C. The Absorption Spectrum of Diborane. *J. Chem. Phys.* **1948**, *16*, 894–902.
- (6) Lin, M.-Y.; Lo, J.-I.; Chou, S.-L.; Peng, Y.-C.; Lu, H.-C.; Cheng, B.-M.; Ogilvie, J. F. Vacuum-Ultraviolet Photolysis of Methane at 3 K: Synthesis of Carbon Clusters up to C₂₀. *J. Phys. Chem. A* **2014**, *118*, 3438–3449.
- (7) Lu, H.-C.; Peng, Y.-C.; Lin, M.-Y.; Chou, S.-L.; Lo, J.-I.; Cheng, B.-M. Photoluminescence of a CVD Diamond Excited with VUV Light from a Synchrotron. *Opt. Photonics J.* **2013**, *3*, 25–28 and references therein.
- (8) Frisch, M. J.; Trucks, G. W.; Schlegel, H. B.; Scuseria, G. E.; Robb, M. A.; Cheeseman, J. R.; Scalmani, G.; Barone, V.; Mennucci, B.; Petersson, G. A. et al. *Gaussian 09*; Gaussian, Inc.: Wallingford, CT, 2009.
- (9) Dalton, a program for molecular electronic structure, release DALTON2014.alpha, 2014, cf. <http://daltonprogram.org>.
- (10) Koizumi, H.; Yoshimi, T.; Shinsaka, K.; Ukai, M.; Morita, M.; Hitano, Y. VUV-Optical Oscillator Strength Distributions of C₃H₆ and C₄H₈ Isomers. *J. Chem. Phys.* **1985**, *82*, 4856–4861.
- (11) Cheng, B.-M.; Chen, H.-F.; Lu, H.-C.; Chen, H.-K.; Alam, M. S.; Chou, S.-L.; Lin, M.-Y. Absorption Cross Section of Gaseous Acetylene at 85 K in Wavelength Range 110–155 nm. *Astrophys. J., Suppl. Ser.* **2011**, *196*, 3.
- (12) Ogilvie, J. F.; Chou, S.-L.; Lin, M.-Y.; Cheng, B.-M. Mid-Infrared Spectra of Methane Dispersed in Solid Ne and Ar. *Vib. Spectrosc.* **2011**, *57*, 196–206.
- (13) Peiser, H. S. X-ray Diffraction Studies and their Crystal-Chemical Implications. In *Formation and Trapping of Free Radicals*; Bass, A. M., Broida, H. P., Eds.; Academic Press: New York, 1960; Chapter 9.
- (14) Robin, M. B. *Higher Excited States of Polyatomic Molecules*; Academic Press: New York, 1985.